International Journal of Scientific & Engineering Research, Volume 4, Issue 1, January-2013
ISSN 2229-5518

RF MEMS Double Beam Lateral Switch Characteristics Analysis Using Neural Network

S.Suganthi, K.Murugesan and S.Raghavan

Abstract— This paper presents Artificial Neural Network (ANN) implementation for Mechanical modeling of Radio Frequency Micro Electro Mechanical System (RF MEMS) lateral double beam switch. We propose an efficient approach based on ANN for analyzing the static and dynamic characteristics of RF MEMS lateral switch by calculating its characteristics parameters. ANN model were trained with five learning algorithms and the results from the neural model trained by Levenberg-Marquardt back propagation algorithm are highly agreed with theoretical results. The neural network shows better results with highest correlation coefficient (0.5844) along with lowest root mean square error (0.0539).

Index Terms— Artificial neural networks, Micro electro mechanical systems, threshold voltage, frequency response and effective mass.

1 INTRODUCTION

Micro Electro Mechanical System (MEMS) is the integration of mechanical elements, sensors, actuators and electronics on common silicon substrate by micromachining process [1]. The advancements in the field of designing sensors, micro machines and control elements have facilitated much attention in the rapid developments of radio frequency (RF) MEMS. The first MEMS switch was demonstrated in 1971 using electrostatic actuation used to switch low frequency electrical signals [2]. When compared to the performance of MEMS switches, traditional integration of PIN diode and GaAs FET in switching circuits is degraded because of high insertion and low isolation losses in high frequency (GHz) [3]. They are suffering from high power consumption and significant inter modulation product due to nonlinear characteristics [4].

On the other hand, the recently developed RF MEMS switches exhibit excellent switching characteristics over wideband from RF to mm–wave frequencies (0.1 to 100GHz) with the following remarkable advantages such as extremely low insertion loss (0.1dB) and very high isolation upto 100GHz, near zero power consumption (10-200nJ/switching cycles), simple biasing circuit, potential for low cost and no inter modulation product (30-50dB better than PIN or FET switches) [4, 5].

Based on direction of motion, MEMS switches can be classified as vertical and lateral switches. Most of the reported works are based on vertical switch which performs in wafer plane displacement and surface contact [6]. But the lateral switch performs in wafer plane displacement and side wall contact. The vertical switches have the drawbacks of stiction problem during the moveable structure release. But in the case of lateral switches, the actuators, contacts, support structures and conducting paths can be fabricated in a single step and hence have the benefit of co-fabrication. Besides, it is easy to get mechanical force in opposing direction even when electrostatic designs are used [6, 7].

The superior qualities of RF MEMS switches make them as viable structure for various applications such as signal routing in transceivers applications [8], phase shifters in phase array antenna [3], impedance matching networks [6], wide band tuning networks, reconfigurable antennas, filters and related circuits [9]. MEMS concepts have been successfully applied in the development of RF switches to be used in the phase shifters which are having the benefits of low loss, low parasitic capacitance and high linearity [10]. In order to analyze and optimize the design of these complex structures, several techniques have been proposed in the past decade. Softwares based on Electromagnetic and Electromechanical [11] principles are also developed for commercial use. But these techniques are not much suitable for modeling of RF MEMS devices due to much computational time and efforts involved.

An accurate device characterization and efficient prediction of general input-output relationship can be achieved based on nonlinear mapping capabilities of Artificial Neural Network (ANN) [12]. ANNs have been utilized for modeling of integrated circuits in RF and millimeter wave frequency range [13]. In this work, threshold voltage and frequency response of a cantilever bean used in the double beam lateral switch which find application in high frequency transmitting and receiving signal routing has been analyzed using neural networks. Generation of training and testing datasets are realized from MATLAB simulation. The cantilever beam used in the switch has been analyzed in terms of it static threshold voltage and dynamic frequency response and effective mass. Due to the optimization of generalized dimension of actuation part, the datasets for the mechanical design of the switch are obtained. The resultant input and output relationship are mapped using the neural model. Based on valid range of input parameters, neural networks are trained and tested. The neural models are trained with Levenberg-Marquart (LM), Bayesian Regularization (BR), Quasi – Newton (QN), Scaled Conjugate Gradient

- *S.Suganthi is currently doing her research in the firled of RF MEMS in Anna University, Chennai, India. E-mail:sugi19770@yahoo.com*
- *Dr.K.Murugesan is currently working as Professor in Sree Sastha Institute of Engineering and Technology, Chennai, India.*
- *Dr.S.Raghavan is currently working as Professor in National Institute of Technology, Trichy, India.*

(SCG) and Conjugate Gradient of Fletcher – Powell (CGF) training algorithms. Although extensive time and effort are required for preparing the dataset, once the network is trained, the proposed model accurately predicts the device responses for arbitrary inputs within the desired range.

2 Theory of Double Beam Lateral RF MEMS Switch

The detailed loss analysis of single beam lateral switch was discussed with ON and OFF states in our previous work [13]. In this paper, double beam RF lateral switch consisting of a Si-core finite ground coplanar waveguide (FGCPW) and an electrostatic actuator is designed as shown in fig.1 for ANN implementation since it provides low insertion loss and high power handling. FGCPW is formed by thick single-crystal-silicon plate that has been coated with thin layer of aluminum to make the RF signal propagation not only along the metal on the top surface, but also on the sidewalls of the transmission line. In this switch, two cantilever beams are employed and can be used as signal lines together to propagate RF signal [14]. Both the fixed connections of the two cantilever beams are from the same port and the two contact tips are on the other port. At the free-end of the two cantilever beams, both ground lines extend towards the nearby cantilever beams to serve as their fixed electrodes respectively.

When sufficient DC bias voltage is applied between the cantilever beam and the ground line, the cantilever beam is pulled toward the fixed electrode by electrostatic force until its free end hits the contact tip, resulting in the on-state of the switch. When DC bias voltage is removed, the mechanical stress of the beam overcomes the stiction forces and pulls the cantilever beam away, resulting in the off-state of the switch. Due to the asymmetrical layout of the two ports, the S-parameters obtained from the two ports are not reciprocal [3].

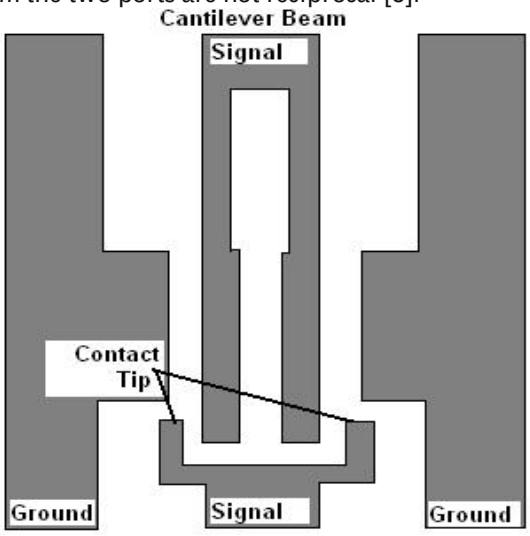

Fig. 1. Schematics top view of Double beam RF lateral switch.

2.1 Mechanical modeling of lateral switch

When a micro machined circuit is designed, it is important to consider the switching voltage required for its operation. The low actuation voltage can be achieved through the optimization of the geometrical dimensions of the actuation part. The top view of the electrostatic actuator used in the modeling is shown in fig.2.

The actuator consists of four components: a suspended cantilever beam serving as a movable electrode, an anchor on the substrate to support the cantilever beam, a fixed electrode opposite to the cantilever beam and a contact tip. The cantilever beam OC is a beam-mass structure. For the beam part OA, the width is w_1 and the length is l_1. For the mass part AC, the width is w_2 and the length is $(l_2 + l_3)$ in which l_2 is the length of the electrode section AB and l_3 is the length of BC. The mass width w_2 is designed to be relatively wider than the beam width w_1 so that low threshold voltage can be maintained and greater deformation of the electrode section may be avoided.

2.2 Static Threshold Voltage

Assuming the electrode part of the cantilever beam is subjected to a uniform load, the equivalent stiffness k of the cantilever beam can be derived by the expression [15]

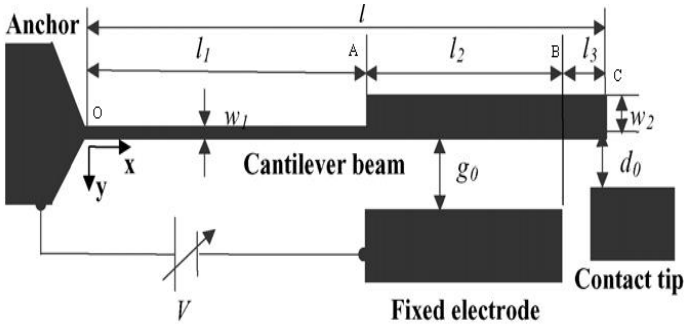

Fig. 2. Top view of the electrostatic actuator

$$k = \frac{12E_1E_2I_1I_2}{\left[\left(\frac{3}{2}l_2^3 + 2l_2^2l_3\right)E_1I_1 + \left(4l_1^3 + 9l_2l_1^2 + 6l_1l_2^2 + 6l_1^2l_3 + 6l_1l_2l_3\right)E_2I_2\right]} \quad (1)$$

and E_1 and E_2 are the Young's moduli of the narrow and wide part of the beam respectively. I_1 and I_2 are the moments of inertia of the cross sectional area of the narrow and wide part of the beam respectively .We assume that

$$E_1 = E_2 = E_{si} = 140GPa. \quad (2)$$

$$I_1 = \frac{1}{12}w_1^3 t$$

$$I_2 = \frac{1}{12}w_2^3 t \quad (3)$$

Where E_{si} is the Young's modulus of the single-crystal-silicon (140 GPa) and t is the height of the cantilever beam. After the deposition of aluminium on the top surface of the beam, it becomes the beam made of single crystal silicon partially cov-

ered with aluminium. Therefore E_1, E_2, I_1 and I_2 can be given by

$$E_1 = \frac{E_{si} w_1 + 2E_{Al} w_{Al}}{w_1 + 2w_{Al}} \tag{4}$$

$$I_1 = \frac{1}{12}(w_1 + 2w_{Al})^3 t \tag{5}$$

$$E_2 = \frac{E_{si} w_1 + 2E_{Al} w_{Al}}{w_2 + 2w_{Al}} \tag{6}$$

$$I_2 = \frac{1}{12}(w_2 + 2w_{Al})^3 t \tag{7}$$

where E_{Al} is the Young's modulus of aluminium coated portion of beam (70GPa), w_{Al} the thickness of aluminium deposited at sidewalls of the silicon beam. Distance between the ends of two electrodes g and the threshold voltage V can be related by solving the equation $F_e(g) = F_r(g)$ where

$$F_e(g) = \frac{\varepsilon_0 I_2 t V^2}{2g^2} \tag{8}$$

$$F_r(g) = k(g_0 - g) \tag{9}$$

are the electrostatic and restoring forces respectively with ε_0 is the permittivity of the air $(8.854\, X\, 10^{-12}\ F/m)$.

2.3 Dynamic frequency response

The frequency response of the cantilever beam is useful to determine the switching time and the mechanical bandwidth of the lateral switch [14]. Using Laplace transform, the frequency response of the cantilever beam with small vibration amplitude can be obtained as

$$\frac{Y(j\omega)}{F(j\omega)} = \frac{1/k}{1 - (\omega/\omega_0)^2 + j\omega/(Q\omega_0)} \tag{10}$$

where Y is the lateral displacement of the cantilever beam relative to the origin of the fixed electrode, F is the electrostatic force, ω is the working angular frequency, k is the effective stiffness, ω_0 is the natural resonant angular frequency and Q is the quality factor of the cantilever beam. ω_0 and Q are expressed as

$$\omega_0 = \sqrt{k/m} \tag{11}$$

$$Q = k/(\omega_0 b) \tag{12}$$

where m and b are the effective mass and damping coefficient of the simplified system . The quality factor Q of the cantilever beam is determined by several variables such as the pressure, the temperature and the intrinsic material dissipation. The quality factor is also an important component for the switching time calculation.

where m and b are the effective mass and damping coefficient of the simplified system . The quality factor Q of the cantilever beam is determined by several variables such as the pressure, the temperature and the intrinsic material dissipation. The quality factor is also an important component for the switching time calculation.

2.4 Dynamic effective mass

It is noted that the effective mass of the cantilever beam is not equal to the actual mass of the cantilever beam since only the end portion of the cantilever beam is moving [14]. Assume the cantilever beam is subjected to a concentrated load P at the center of the electrode section of the cantilever beam. Based on fig.2, we can consider the displacement y_k and kinetic energy E_k of the cantilever beam at three portions, respectively.

The first part is the length of the beam ranging $0 \le x \le l_1$. Its kinetic energy E_{k1} is given by

$$E_{k1} = \frac{1}{2} m_1 \left(\frac{P}{2E_1 I_1}\right)^2 \left(\frac{-4l_1^4 + 25l_1^3 l_2 + 10l_1^2 l_2^2}{30}\right) \tag{13}$$

Where $m_1 = (\rho_{si} w_1 + 2\rho_m w_m) l_1 t$ (14)

The second part is from the beginning of the electrode to the center of the electrode of the cantilever beam $(l_1 < x \le (l_1 + l_2/2))$. The kinetic energy E_{k2} is given by

$$E_{k2} = \frac{1}{2} m_2 \left[\left(\frac{P}{E_1 I_1}\right)^2 \frac{l_1^2 (l_1 + l_2)^2}{8} + \frac{P^2}{E_1 I_1 E_2 I_2} \frac{l_1 l_2^2 (l_1 + l_2)}{24} + \left(\frac{P}{E_2 I_2}\right)^2 \frac{49 l_2^4}{5760} \right] \tag{15}$$

Where $m_2 = (\rho_{si} w_2 + 2\rho_m w_m) l_2 t$ (16)

The third part is from the center of the electrode to the end of the cantilever beam $(l_1 + l_2/2 < x \le l_1 + l_2 + l_3)$. The kinetic energy E_{k3} is given by

$$E_{k3} = \frac{1}{2} m_2 \left(\frac{P(l_1^2 + l_1 l_2)}{2E_1 I_1} + \frac{P l_2^2}{8E_2 I_2}\right)^2 \left(\frac{1}{2} + \frac{l_3}{l_2}\right) \tag{17}$$

Therefore, the total kinetic energy E_k is given by

$$E_k = E_{k1} + E_{k2} + E_{k3} = \frac{1}{2} m y_m^2 \tag{18}$$

where the velocity y_m at the end of the cantilever beam is

$$y_m = \frac{P(l_1^2 + l_1 l_2)}{2E_1 I_1} + \frac{P l_2^2}{8E_2 I_2} \tag{19}$$

3 ARTIFICIAL NEURAL NETWORKS

ANNs are biologically inspired computer programs to simulate the way in which the human brain process information. It is a very powerful approach for building complex and nonlinear relationship between a set of input and output data. The recent work by researchers demonstrated the ability of neural networks to learn and model a variety of microwave components, such as micro strip interconnects, spiral conductors, CPW components and packing and interconnects [16]. Neural models can be much faster than original detailed EM/physics models, more accurate than polynomial and empirical models, allow more dimensions than table lookup models and are easier to develop when a new device /technology is introduced [17]. The cost for developing neural models is mainly depending on data collection and training.

The power of computation is determined from connections in a network. Each neuron has weighted inputs, simulation function, transfer function and output. The weighted sum of inputs constitutes the activation function of the neurons. The activation signal is passed through a transfer function which introduces non-linearity and produces the output. During training process, the inter-unit connections are optimized until the error in prediction is minimized. Once the network is trained, new unseen input information is entered into the network to calculate the test output. Many types of neural networks developed for various applications are available in the literature.

The class of neural network and its architecture for a particular model implementation depend on the nature of problem to be solved. The neural network architecture used in this paper is the MultiLayer Perceptron Neural Network (MLPNN). These networks having multilayer feed forward architecture composed of layers of computing nodes called neurons [16]. The MLPNN is one of the most extensively used ANN due to its well-known general approximation capabilities and limited complexity.

The MLPNN model used in this work consists of three layers: an input layer, an output layer and two intermediate or hidden layers. Each neuron in the input layer is acting only as a buffer for distributing the input signals x_i to neurons in the hidden layer. Each neuron j in the hidden layer sums up its input signals x_i after weighting them with the strengths of the respective connections w_{ij} from the input layer and compute its output y_j as a function of the summation and hence

$$y_j = f\left(\sum w_{ij} x_i\right) \quad (20)$$

where f can be a simple threshold function, a sigmoidal [17] or hyperbolic tangent function [18]. The output of neurons in the last (output) layer is computed similarly.

Training a network consists of adjusting weights of the network using learning algorithms. During learning process, neural network adjusts the weights and thresholds so that the error between neural predicted output and sampled output is minimized. All learning algorithms used in this work are based on multilayer correction [19] learning algorithm called back propagation. The five different training algorithms we used in this work are described briefly as below.

3.1 Levenberg – Marquardt (LM) Algorithm

This is a least –square estimation method based on the maximum neighborhood idea [20]. The LM method combines the best features of the Gauss-Newton technique and the steepest-descent method, but avoids many of their limitations. In particular, it generally does not suffer from the problem of slow convergence.

3.2 Bayesian Regularization (BR) Algorithm

This algorithm updates the weight and bias values according to their LM optimization and minimizes a linear combination of squared errors and weights, and then determines the correct combination so as to produce a well generalized network. This algorithm can train any network as long as its weight, inputs and transfer functions have derivative functions [21].

3.3 Quasi-Newton (QN) Algorithm

This is based on Newton's method but doesn't require calculation of second derivatives. An approximate Hessian matrix is updated. At each iteration of the algorithm, the update is computed as a function of the gradient. The line search function is used to locate the minimum [22]. The first search direction is the negative of the gradient of performance. In succeeding iterations the search direction is computed according to the gradient.

3.4 Conjugate Gradient of Fletcher-Reeves (CGF) Algorithm

This method updates weights and bias values according to the conjugate gradient with Fletcher-Reeves. Each variable is adjusted to minimize the performance along the search direction. The line search is used to locate the minimum point. Fletcher-Reeves version of conjugate gradient uses the norm square of previous gradient and the norm square of the current gradient to calculate the weights and biases [22].

3.5 Scaled Conjugate Gradient (SCG) algorithm

This algorithm can train any network as long as its weights, net inputs and transfer functions have derivative function. This algorithm is based on conjugate directions but does not perform line search at each iteration. This was designed to avoid the time consuming line search.

4 PROPOSED ANN MODEL

Two back propagation feed forward ANN architectures (ANN-S for static threshold voltage and ANN-D for dynamic frequency response and mass analysis) are proposed for analysis in this paper and are shown in fig 3(a) & (b). All model parameters are allowed to vary and MATLAB simulation is used to generate the datasets for ANN models. The circuit parameters and dimension of actuated part are selected as input and threshold voltage is the output for ANN-S while length ratio, w_2, Q and frequency of operation are input and frequency response and effective mass are the outputs for ANN-D.

The selected ranges of input parameters used in the netwrok for training are given as follows: $0.1 \le \left(l_1/l_1 + l_2\right) \le 0.95$, $4\mu m \le g_0 \le 10\mu m$, $2\mu m \le w_1 \le 5\mu m$ and $2.5\mu m \le w_2 \le 20\mu m$ for ANN-S and $01. \le Q \le 3$, $0.1KHz \le f \le 100KHz$ and

$440\mu m \le (l_1 + l_2) \le 540\mu m$ for ANN-D respectively. The ratio of training to test data records employed in the experiment is 60:20. This means that with 468 data records, there are 280 records for the training set and 94 records for the test set. The chosen best trained Levenberg-Marquardt algorithm uses input vectors and corresponding target vectors to train the neural networks. The number of hidden units directly affects the performance of the network. Therefore, many experimental investigations are conducted. The number of hidden nodes determined to provide the optimal result are 10 for first and 6 for second hidden layers respectively.

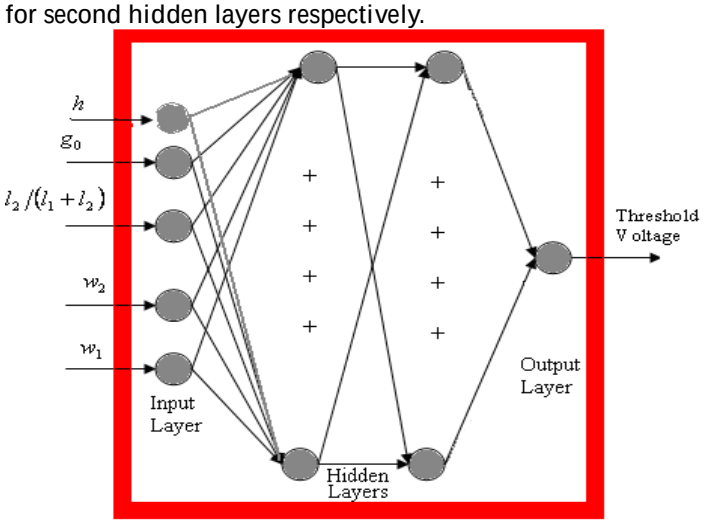

(a)

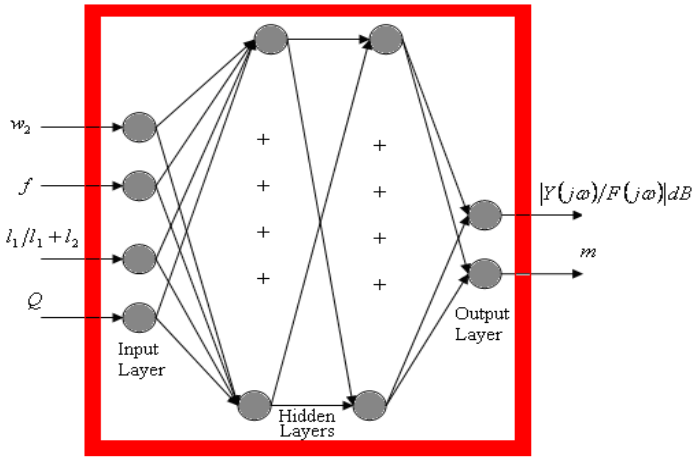

(b)

Fig.3. Feed forward ANN architecture for (a) Static (b) Dynamic behavior of double beam switch

Thus the architecture of network obtained is 5-10-10-1 for ANN-S and 4-6-6-2 for ANN-D. The number of input nodes is 5 and 4 for ANN-S and ANN-D respectively, representing the geometrical parameters of the switch that affect outputs. The numbers of output nodes are 1 and 2 for ANN-S and ANN-D respectively. In order to evaluate the performance of the ANN models, the mean square error (MSE) and the correlation coefficient (R^2) as defined below are calculated in terms of the difference between the output of ANNs and training datasets:

$$MSE = \frac{1}{N}\sum_{x=1}^{N}(\hat{x}_i - x_i)^2 \tag{22}$$

$$R^2 = 1 - \frac{\sum_{i=1}^{N}(\hat{x}_i - x_i)^2}{\sum_{i=1}^{N}(x_i - \bar{x}_i)} \tag{23}$$

where N is the total number of data sets, $\hat{x}_i$ is input dataset, x_i is trained ANN output and $\bar{x}_i$ is mean of x_i.
where N is the total number of data sets, $\hat{x}_i$ is input dataset, x_i is trained ANN output and $\bar{x}_i$ is mean of x_i.

5 RESULTS AND DISCUSSION

In order to obtain better performance, faster convergence and a simpler structure, the proposed ANN as shown in fig.3 was trained with five different training algorithms. To prove the efficiency and accuracy of the developed ANN models, the selected range of input values are used and the networks are validated. The comparison of threshold voltage V_{th} as a function of original gap between two electrodes, g_0 and the beam width w_1 are depicted in fig.4 (a) and (b) for ANN model and simulation .

It is obvious from fig 4 (a) that the threshold voltage V_{th} decreases when the original gap between the two electrodes g_0 decreases or the length sum $(l_1 + l_2)$ increases. When the cantilever beam length ratio $l_2/(l_1 + l_2)$ is within the range of 30–75 %, V_{th} only changes within 10% of the minimum value of V_{th} which is referred to as V_{th} (min). The corresponding length ratio $[l_2/(l_1 + l_2)$ min1 +l2)](min) to V_{th} (min) is 50% when $w_1 = 2.4\mu m, w_2 = 5\mu m$ and $w_{Al} = 0$.

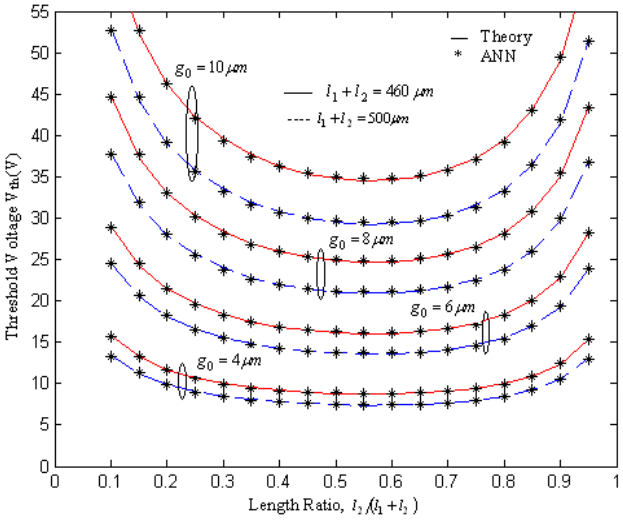

(a)

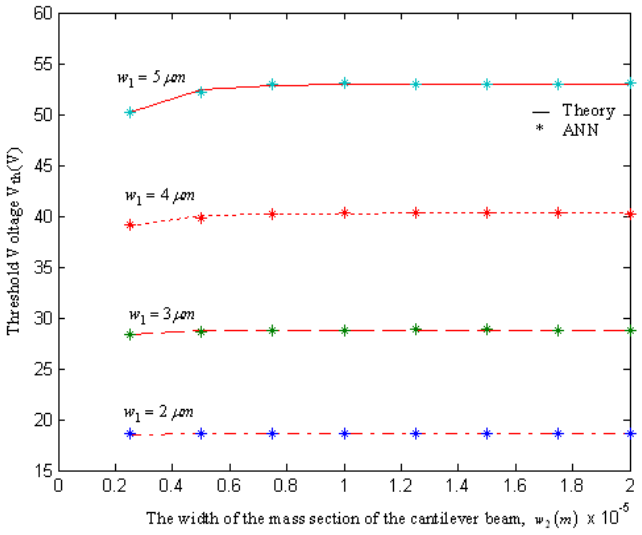

(b)

Fig.4.Comparision of ANN and simulation results of calculated threshold voltage V_{th} (a) with various lengths $(l_1+l_2), l_2/(l_1+l_2)$ ratio, and initial gap distance g_0 $l_3=10\mu m$, $w_m=0$, $w_2=5\mu m$ and $w_1=2.4\mu m$ (b) with various cantilever beam widths (w_1, w_2) $(l_1=275\mu m, l_2=165\mu m)$.

It also shows that $l_2/(l_1+l_2)$(min) is almost independent of the initial gap g_0 and the length sum (l_1+l_2). Figure 4 (b) shows that the threshold voltage V_{th} is more dependent on the beam width w_1 than the mass width w_2. The effect of the mass width w_2 is negligible. The threshold voltage V_{th} increases with beam width w_1.

In the fig 5 (a), the variation in the frequency response of the cantilever beam is simulated with different quality factors. It shows that the response amplitude at 15 kHz is increased when the quality factor ranges from 0.2 to 2.0. When $Q \le 0.5$, it has a slow switching time; when $Q \ge 2$, it has a long settling time. In practice, it is beneficial for the switching time that the quality factor of the cantilever beam is designed by $0.5 \le Q \le 2$.

Figure 5(b) reveals the portion mass m_1, m_2 and the effective mass m of a cantilever beam changes with the ratio of $l_2/(l_1+l_2)$ when $l_3=10\mu m$ and $l_1+l_2=440\mu m$. It is found that the effective mass m is mainly determined by the mass of the electrode part m_2. The effective mass m is 5–85% of the actual total mass of the cantilever beam $[m_1+m_2(1+l_3/l_2)]$ when the ratio of $l_2/(l_1+l_2)$ is within the range of 30–75%.

Figure 5(c) shows that the natural resonant frequency of the cantilever beam changes with the ratio of $l_2/(l_1+l_2)$ and the sum of (l_1+l_2). It shows that the natural resonant frequency of the cantilever beam does not changes significantly when $l_2/(l_1+l_2)$ is within the range of 30–75%. For example, with $l_3=10\mu m$ and $l_1+l_2=440\mu m$, the resonant frequency is 15 ± 0.5 kHz when $l_2/(l_1+l_2)$ is varying in the range of 0.3–0.75. The natural resonant frequency of the cantilever beam decreases with the increase of (l_1+l_2) due to the increase of the effective mass and the decrease of the stiffness of the cantilever beam.

Two parameters namely correlation coefficient and Mean Square Error (MSE) values are used for the performance evaluation of the models and comparison of the results for prediction of S-parameters. The higher value of correlation coefficient and a smaller value MSE mean a better performance of the model. The results of the neural network based modeling of S-parameter calculation of different combination of input parameters with the used data set are provided in Tables 1 in terms of the correlation coefficient and mean square errors. From fig.4 &5 and the table 1, it is observed that there is an excellent agreement between the ANN & theory result.

TABLE.1

CALCULATED MEAN SQUARE ERROR (MSE) &CORRELATION COEFFICIENT (R^2) OF MASS & RESONANT FREQUENCY CALCULATION

parameters	Mass calculation		
	$m\ (ng)$	$m_1\ (ng)$	$m_2\ (ng)$
MSE	2.9722e-019	3.0709e-020	1.2087e-020
R^2	0.1375	0.17974	0.2446
parameters	Resonant frequency calculation $(l_1+l_2)(\mu m)$		
	440	500	540
MSE	5.7846e-004	5.4444e-004	0.0539
R^2	0.4057	0.5844	0.1790

The above table shows that the neural network provides better results in terms of the higher correlation coefficient, which measures the strength and direction of the linear relation between two variables (actual and predicted values) of R^2=0.2446 (0.5844) with minimum mean square error (MSE) of the model of 1.2087e-020 (0.0539) for threshold voltage calculation in terms of various length ratios and beam widths.

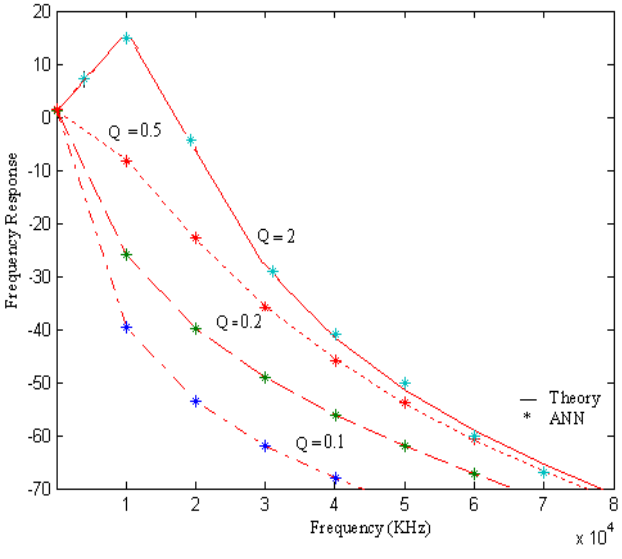

(a)

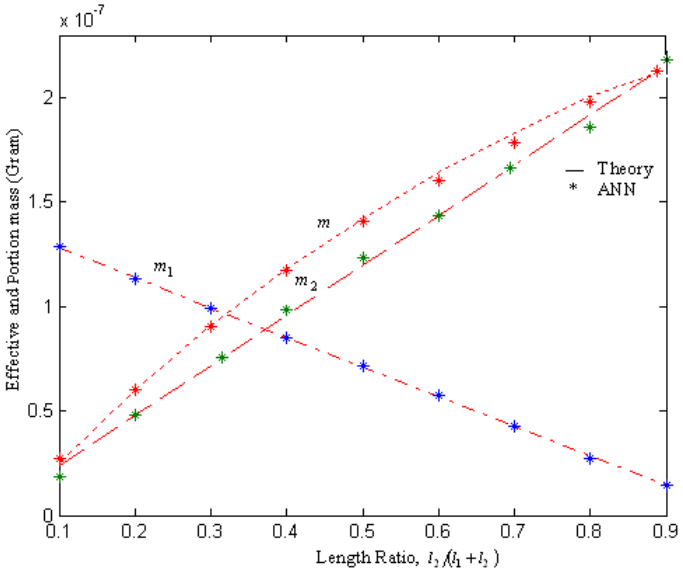

(b)

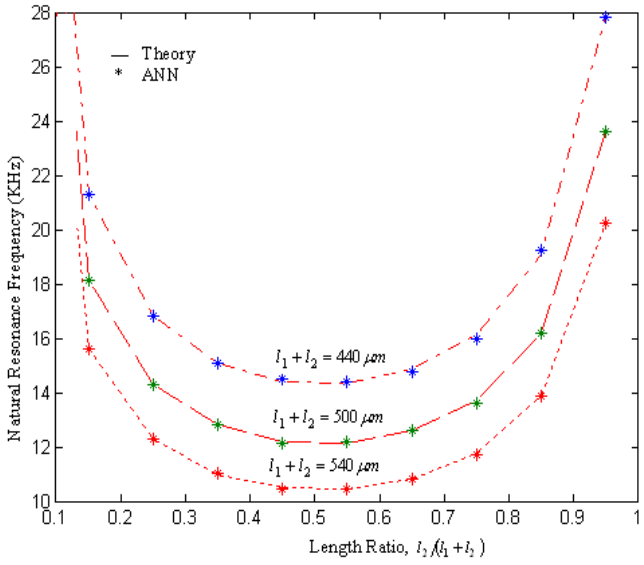

(c)

Fig5. Comparison of ANN and simulated results of (a) Frequency response of a cantilever beam with resonant frequency $f=15KHz$ and $k=0.94$ (b) Effective mass and portion mass of the cantilever beam versus the ratio of $l_2/(l_1+l_2)$ for $w_1=2.4\mu m$, $w_2=5\mu m$, $l_1+l_2=440\mu m$, $l_3=10\mu m$, $w_{Al}=0.6\mu m$ and $h=35\mu m$. (c) Natural resonant frequency versus the ratio of $l_2/(l_1+l_2)$ for $w_2=5\mu m$, $h=35\mu m$ and $w_1=2.4\mu m$, $w_{Al}=0.6\mu m$.

6 CONCLUSION

We have made a comprehensive analytical model based on MLP neural network for the design of static and dynamic lateral RF MEMS switch. The developed neural model matches closely with the literature results. The proposed ANN structure can be effectively used for analyzing the characteristics of lateral RF MEMS switch based on static and dynamic behavior. The comparison between the neural model and theoretical results reveals that our proposed neural model is much useful for the behavior study of RF lateral double beam switches. Since the neural models presented in this work have good accuracy, require no tremendous computational efforts and less background information about bridges, they can be very useful for the development of fast CAD algorithms. A distinct advantage of neural computation is that, after proper training, a neural network completely bypasses the repeated iterative processes when new cases are presented to it. Since the training and testing time is less than few microseconds, the proposed neural model is quite fast in the design and loss analysis of lateral MEMS series switch.

REFERENCES

[1] Muldavin J B and Rebeiz G M, High isolation MEMS shunt switches part 1: Modeling, IEEE Trans Microwave Theory Tech (2000), 1045-1052.

[2] C.Goldsmith, J.Ramtall, S.Eshelman, T.H.Lin and D.Demision, Characteristics of micro machined switches at microwave frequencies, Proceedings of the IEEE MTT-S Dig (1996), 1141–1144.

[3] M. Tang, A.-Q. Liu, A. Agarwal and Z.-S. Liu, C. Lu, single-pole double-throw (SPDT) circuit using lateral metal-contact micro machined switches, IEEE Trans Sensors and Actuators (2005), 187–196.

[4] Mohammad N. Mollah and Nema1 C. Karmakar, RF- MEMS Switches: Paradigms of Microwave Switching, Proc of APMC200 1, Taipei, Taiwan (2001), 1024-1027.

[5] Gabriel M. Rebeiz, RF MEMS Switches: Status of the Technology, Proc of the 12th Int Conf on Solid State Sensors, Actuators and Microsystems, Boston (2003) 1726-1729.

[6] A Q Liu1, M Tang, A Agarwal and A Alphones, Low-loss lateral micro machined switches for high frequency applications, J Micromechanics and Micro engineering (2005), 157–167.

[7] Hah D, Yoon E and Hong S, A low-voltage actuated micro machined microwave switch using torsion springs and leverage, IEEE Trans. Microwave Theory Tech (2000), 2540–2545.

[8] G. M. Rebeiz, RF MEMS- Theory, Design and Technology (2003), John Wiley and Sons, Hoboken.

[9] Elliot R. Brown, RF-MEMS switches for reconfigurable integrated circuits, IEEE Trans. Microwave Theory Tech (1998), 1868-1880.

[10] B.Lakshanarayana and T.Weller, Distributed MEMS phase shifters on silicon using tapered impedance unit cells, IEEE MTT-S Digest (2002) 1237-1240.

[11] Shyh-Chiang, Low actuation voltage RF MEMS switches with signal frequencies from 0.25 GHz to 40 GHz, IEDM Technical Digest, Electron Devices Meeting (1999), 689-692.

[12] Yongjae Ice,Yonghwa Park,Feng Niu and Dejan Filipovic, Artificial neural network based macro modeling approach for two port RF MEMS resonating structures, IEEE Trans. Microwave Theory and Tech (2005), 261-266.

[13] S.Suganthi, K.Murugesan and S.Raghavan, Neural network based realization and circuit analysis of lateral RF MEMS series switch, Proc. of IEEE International Conference on Computer, Communication and Electrical Technology (2011), 260-265.

[14] Ai Qun Liu, Aibin YuMing Tang, Muhammad Faeyz Karim and Selin Teo Hwee Gee, RF MEMS switches and integrated switching circuits-Design, fabrication and test (2010), Springer MEMS reference shelf.

[15] Gere J M and Timoshenko S P, Mechanics of material (1997), 4th edition.

[16] Gregory L. Creech, Bradley J. Paul, Christopher D. Lesniak, Thomas J. Jenkins and Mark C. Calcatera, Artificial neural networks for fast and accurate EM-CAD of microwave Circuits, IEEE Trans. Microwave theory Tech (1997), 1794 -802.

[17] Younjae Lee and dejan S Filipovic, ANN based electromagnetic models for the design of RF MEMS switches, IEEE Microwave and Wireless components Letters (2005), 823-825.

[18] Zaabab, Q. Zhang, and M. Nakhla, Analysis and optimizations of microwave circuits and devices using neural networks models, IEEE MTT-S Dig, San Diego, CA (1994), 393 -396.

[19] S. Haykin, Neural Networks, A comprehensive foundation (1994), Macmillan College Publishing Comp.

[20] K. Levenberg, Method for the solution of certain nonlinear problems in least squares, Quart. Appl (2004), 164-168.

[21] D.J.C. MacKay, Bayesian interpolation - Neural Computation (1992), 415-447.

[22] C. Yildiz and M. Turkmen, A CAD approach based on artificial neural networks for shielded multilayered coplanar waveguides, AEU Int J of Elect. And Com (2004), 284-292.